Satellite data reveal southwestern Tibetan Plateau cooling since 2001 due to snow-albedo feedback

Donglin Guo[1,2], Jianqi Sun[1], Kun Yang[3], Nick Pepin[4], Yongming Xu[5], Zhiqing Xu[6,1], Huijun Wang[2]

1. Nansen-Zhu International Research Centre, Institute of Atmospheric Physics, Chinese Academy of Sciences, Beijing, China
2. Key Laboratory of Meteorological Disaster, Ministry of Education/Collaborative Innovation Center on Forecast and Evaluation of Meteorological Disasters, Nanjing University of Information Science & Technology, Nanjing 210044, China
3. The Ministry of Education Key Laboratory for Earth System Modeling, Department of Earth System Science, Tsinghua University, Beijing, China
4. Department of Geography, Buckingham Building, Lion Terrace, University of Portsmouth, United Kingdom
5. School of Remote Sensing and Geomatics Engineering, Nanjing University of Information Science and Technology, Nanjing, China
6. Climate Change Research Center, Chinese Academy of Sciences, Beijing, China

This article has been accepted for publication and undergone full peer review but has not been through the copyediting, typesetting, pagination and proofreading process which may lead to differences between this version and the Version of Record. Please cite this article as doi: 10.1002/joc.6292

*Corresponding author:

Donglin Guo, NZC, Institute of Atmospheric Physics, Chinese Academy of Sciences, P. O. Box 9804, Beijing 100029, China

E-mail: guodl@mail.iap.ac.cn

Key points:

- It is found that the southwestern Tibetan Plateau cools recently against an overall warming over the rest of the Plateau
- Enhancement of snow-albedo feedback is responsible for the cooling over the southwestern Tibetan Plateau
- Climate change in the southwestern Tibetan Plateau and its surroundings supports the abnormal 2 m air cooling

Abstract

Given the threats that climate change poses to solid water reservoirs on the Tibetan Plateau (TP), there is significant interest in understanding spatial patterns of climate change and their causes. Weather station observations have been extensively examined, but are scarce, resulting in an incomplete understanding of climate change across the TP, particularly in the west. Using recent (2001–2015) satellite-based data

sets (2 m air temperature, land surface temperature, albedo and snow cover), this study reveals that mean annual 2 m air temperature in the southwestern TP has decreased by 0.15 °C decade^{-1} in contrast to overall warming (+0.18 °C decade^{-1}) on the rest of the TP. Up to 45% (74%) of the variance in the annual (spring) 2 m air temperature can be explained by simultaneous change in snow-induced albedo in the southwestern TP. The free atmosphere column over this region and Northwest India is cooling, providing a favorable environment for the decrease in 2 m air temperature observed. Moreover, the anomalous water vapor transport into the southwestern TP is advantageous for increased snowfall and the associated decrease in 2 m air temperature. The implications of this anomalous cooling under global warming have yet to be fully considered, in particular for the futures of glaciers and snowpack over the Himalayan Mountains in the southwestern TP.

Key words: Tibetan Plateau; Climate warming; Snow-albedo; Anomalous cooling

1. Introduction

The Tibetan Plateau (TP) is a significant source of water resources in the form of snow and ice. It is the highest (> 4000 m on average) and the most extensive (approximately 2.5×10^6 km^2) highland in the world. Cold conditions facilitate the formation of considerable solid water resources [~1.0×10^5 km^2 of glaciers (Yao *et al.*,

2012a), ~41.9 × 10^9 m^3 $year^{-1}$ water equivalent of snow (Li *et al.*, 2008), and ~ 1.1 × 10^6 km^2 of permafrost (Zou *et al.*, 2017)]. These feed the major rivers in East Asia, South Asia, and Southeast Asia (Indus, Ganges, Brahmaputra, Mekong, Yangtze, and Yellow Rivers) and provide water to more than 1.4 billion people (Immerzeel *et al.*, 2010; Yao *et al.*, 2012a). The TP is thus praised as the 'Asian water tower' (Kang *et al.*, 2010).

The fate of these solid water resources is linked to climate change. Owing to the location in mid and low latitudes, much of the water resource is relatively warm and therefore sensitive to climate warming compared with that in high latitudes (Yao *et al.*, 2012b; Guo and Wang, 2016; Yan *et al.*, 2018). An integrated assessment of glacier status on the TP and its adjacent regions showed that 55 of 82 glaciers have shrunk over the past 30 years (Yao *et al.*, 2012b). The TP permafrost has degraded, characterized by a rise in soil temperature (Yao *et al.*, 2012b), a reduction in permafrost area (Guo and Wang, 2013), and a thickening of the active layer (Guo and Wang, 2013). Since the early 1980s, snow depth and the number of snow cover days have decreased and the duration of snow cover has shortened (Xu *et al.*, 2017).

Accurate quantification of temperature change on the TP is essential for effective evaluation of current and future sustainability of the solid water resource. Much research has concentrated on climate warming with respect to the amplitude or rate of

warming (Liu and Chen, 2000; You *et al.*, 2008; Yan *et al.*, 2014), spatial patterns (Yang *et al.*, 2014), seasonality (Guo and Wang, 2012) and elevation-dependent warming (Rangwala and Miller, 2012; Pepin *et al.*, 2015; Cai *et al.*, 2017). However, all such observation-based studies are plagued by the scarcity of observations. In particular, there are only several stations in the whole of the western TP, resulting in great uncertainty across much of the region and a lack of understanding of climate change across the TP as a whole.

The aim of this study therefore is to use recent (2001–2015) comprehensive satellite-based datasets (2 m air temperature, land surface temperature, albedo and snow cover) (in particular 2 m air temperature) to reveal climate change and to attempt to understand its causes for the entire TP at 1 km resolution.

2. Data and methods

Monthly Moderate Resolution Imaging Spectroradiometer (MODIS) land surface temperature (MODIS LST) is used in this study, with the monthly mean calculated based on averaging daytime/nighttime LST from MOD11A1, version 6 (Wan, 2013). The data cover a period 2001–2015 and have a resolution of 1 km. Because MODIS LST is influenced by surface radiative effects, particularly at high elevation (Pepin *et al.*, 2016), it is not the same as screen-level (2 m) air temperature which is commonly

used for climate change assessments (i.e. IPCC, 2013). Therefore, we also used a satellite-based screen-level (2 m) air temperature (SBAT) dataset, which is developed using machine learning models based on MODIS data (LST and NDVI), solar radiation, shuttle radar topography mission (SRTM) digital elevation model (DEM) data, and topographic index data (Xu *et al.*, 2018). The SBAT has a resolution of 1 km across the entire TP and covers the period 2001–2015. While annual MODIS LST has a temporal correlation coefficient of 0.74 with 2 m air temperature observations at 104 weather stations and a much lower temperature trend (2001–2015) than the 2 m air temperature observations (+0.18 vs. +0.27 °C decade^{-1}) (Figure 1), the SBAT is much closer to the 2 m air temperature observations both in correlation (0.94) and mean trend (+0.24 °C decade^{-1}). Thus, we rely mostly on SBAT to examine climate change in this study.

Other satellite-based data used to examine mechanisms of climate change include (i) monthly surface albedo (converted from the 16-day MODIS albedo product MCD43B3, version 5) and (ii) monthly MODIS normalized difference snow index (NDSI, calculated from the daily NDSI product MOD10A1, version 6). The albedo product has been validated in previous studies across the TP (Qin *et al.*, 2011). The NDSI denotes the difference in reflectance monitored in visible and short-wave infrared hands, and it can effectively distinguish snow from other surface features

(Hall *et al.*, 1995; Tang *et al.*, 2013). We use the NDSI data to represent snow cover in this study. Both datasets also have a resolution of 1 km and cover the period 2001–2015.

Monthly 2 m air temperature observations at 104 weather stations are obtained from the China Meteorological Administration. Stations are mostly located in the central and eastern TP (Figure 2). Records from 2001 to 2015 were used to validate the satellite-based data. Data quality control, based on logical testing and comparison with adjacent stations has previously removed unreliable observations (Li *et al.*, 2004; Wang and Zeng, 2018).

Monthly gridded precipitation is obtained from the Global Precipitation Climatology Centre (GPCC) (https://www.esrl.noaa.gov), which is developed based on global weather station data (Schneider *et al.*, 2011). The data cover a period from 1901–2018 and have a resolution of 1°. Monthly snowfall is determined from monthly GPCC precipitation with snowfall occurring when mean monthly SBAT falls below freezing point. These data have also been used previously for research on climate on the TP (Duan *et al.*, 2011).

Monthly gridded free-atmospheric temperature at 12 vertical levels and vertically integrated water vapor from the European Centre for Medium-Range Weather Forecasts Reanalysis Interim (ERA-Interim) (Dee *et al.*, 2011) are used to compare

the free atmospheric profile with surface based conditions, and quantify advection of moisture. Vertical levels include 1000, 950, 850, 700, 600, 500, 400, 300, 250, 200, 150 and 100 hPa. Temperatures (water vapor) are archived at a resolution of 0.125° (0.75°). ERA-Interim has previously been shown to have the best performance amongst many reanalysis data on the TP (Wang and Zeng, 2012).

Finally, global digital elevation data (GTOPO30) were used to quantify surface elevation. They are provided by the U.S. Geological Survey's Center for Earth Resources Observation and Science (http://eros.usgs.gov/), with a resolution of ~1 km. All data sets (SBAT, MODIS-based LST, snow cover and albedo, GPCC and ERA-Interim) were interpolated or resampled to a common resolution of 1 km for comparison. Linear trends of all variables are calculated using the slope of an ordinary least squares regression line, and their statistical significances are evaluated using the Student's *t* test.

3. Results

3.1 The southwestern TP cooling

The SBAT record indicates that a majority of the TP has experienced warming from 2001 to 2015 except for some southwestern areas (outlined by the blue box) (Figure 2). The annual SBAT rate of increase (decrease) is 0.18 (−0.15) °C decade^{-1}

averaged over the entire (southwestern) TP. Anomalous cooling is interesting under in the context of current global warming (Kosaka and Xie, 2013). In addition, the southwestern TP is a critical location due to the inclusion of the Himalayan mountain chains where considerable solid water resources are present (Dimri *et al.*, 2018). Therefore, this study focuses on the southwestern TP. The temperature decrease in the southwestern TP is also demonstrated in MODIS LST data (Figure 3) and in weather station observations (Figure 4) although the latter are very sparse. On a seasonal scale, most of the decrease is concentrated in spring and winter, whereas autumn (summer) SBAT shows an increase (weak decrease) (Figure 2). The annual signal is dominated by winter and spring trends at a time of year when snow cover will be significant across much of the region.

3.2 Forcing mechanisms

Other datasets are examined to illustrate trends in possible forcing mechanisms. Annual surface albedo has increased over much of the southwestern TP, and is strongly negatively correlated to the 2 m air temperature decrease (Figure 5a). The areal mean series have a correlation coefficient of −0.67, so nearly half (45%) of the variance of annual SBAT can be accounted by albedo change (Figure 6). As was the case for SBAT, spring and winter albedo trends are stronger than the annual mean trend (Figure 5c and 5e). For areal mean series, correlation coefficients between

surface albedo and air temperature time series are −0.86 in spring and −0.59 in winter (Figure 6). Thus up to 74% (35%) of the variance in SBAT in spring (winter) can be explained by albedo change.

Snow cover from MODIS has also increased over the southwestern TP, again positively correlated with albedo increase (Figure 5b). For areal mean series, correlation coefficients are 0.98 for the annual mean (Figure 6), and broadly similar values for spring and winter (Figure 5d and 5f, Figure 6). Thus change in albedo is predominantly associated with the change in snow cover. Snow is very efficient at reflecting incoming solar radiation, and thus an increase in snow cover is consistent with the increase in surface albedo. In turn this will encourages 2 m air temperature cooling by subsequently reducing net shortwave radiation (Rangwala and Miller, 2012). Because incoming radiation in spring is much stronger than in winter, it is unsurprising that the correlations between surface albedo and SBAT are strongest then. Taken together these results imply the snow-albedo feedback mechanism is a strong candidate responsible for much of the recent cooling observed over the southwestern TP.

Further analysis suggests that increased snow cover has also been associated with an increase in snowfall (Figure 7), in both in winter and spring. Snowfall is significantly positively correlated with snow cover with coefficients of 0.94 for the

annual mean, 0.78 for spring and 0.63 for winter. The increase in snowfall (as opposed to liquid precipitation) can at least partially be related to the cooling of the free atmosphere surrounding the southwestern TP. Mean annual ERA-Interim free atmosphere temperature over the southwestern TP and Northwest India shows decreasing trends at all heights except 100 hPa (Figure 8). Similar decreases are shown in winter and spring (not shown). ERA-Interim also includes a 2 m air temperature which also decreases over the southwestern TP from 2001 to 2015 (Figure 9), consistent with the decrease of SBAT. This supports the suitable use of ERA-Interim free atmosphere temperature here to some extent. The rapid decrease in free atmospheric temperatures will cool the surrounding environment and be conducive to increased snowfall. However temperature alone is not the sole control. Anomalous water vapor has also been transported into the southwestern TP from southern regions on an annual basis over the trend period (Figure 10a). This is also the case in winter (Figure 10b) and in spring for more eastern and southern regions (Figure 10c). Increased moisture advection is advantageous for increased snowfall, which will enhance the snow-albedo feedback effect and result in decreased SBAT in most elevation bins (Figure 8).

4. Discussions and conclusions

Climate change at high elevations on the TP has gained increasing attention due to its significant influence on both local and regional scale ecosystems, both in the present day and the past (Jin *et al.,* 2005). However, surface observations are lacking and unevenly distributed due to physical challenges in making measurements over rugged and complex terrain (Ma *et al.,* 2008). Using weather stations biased to eastern regions of the TP has been shown to overestimate the warming trend of the plateau as a whole and magnify inter-annual variability in 2 m air temperature (Figure 11). Reanalysis data and model output can expand analysis to the scale of the entire TP, but both have relatively coarse spatial resolution (Wang and Zeng, 2012; Su *et al.*, 2013; Hu *et al.*, 2014; Maussion *et al.,* 2014; Jiang *et al.*, 2016; Gao *et al.*, 2018; Giorgi and Gao, 2018; Guo e*t al.*, 2018). The accuracy of reanalysis data depends on the quantity of surface observations in the region (Dee *et al.,* 2011), and there are therefore known inaccuracies in the reanalyses over the TP (Wang and Zeng, 2012). Satellite monitoring could overcome these inadequacies due to high resolution and regional coverage. Our study uses comprehensive satellite-based datasets (in particular SBAT) to investigate climate change across the whole TP at 1 km resolution. Our study can be considered to be a step forward from research approach perspective.

The southwestern TP, containing the Himalayan mountain chains and adjacent areas, is considered to be topographically representative of many of the typical

features of the TP. These include mountain chains, separated by extensive high elevation plains, with substantial areas of glaciers and semi-permanent snow cover. Thus this area is of great importance for the provision of life-supporting water resources (Dimri *et al.,* 2018). Despite growing research efforts, quantification of climate change is uncertain due to limited observations (Dimri and Dash, 2012; Bajracharya *et al.*, 2015; Waqas and Athar, 2018). Based on 1 km resolution SBAT, MODIS LST and weather station observations, our study reveals a recent cooling trend over much of the southwestern TP. This new finding is supported by concurrent changes in relevant forcing mechanisms, as demonstrated by a wide variety of datasets, including both a moistening and cooling of the free atmosphere and increased snow cover and thus surface albedo.

Our findings are not inconsistent with other recent observational and modelling studies examining past/future profiles of warming, although most studies have only extended their analysis up to around 6000 m. Some of these studies examine patterns of warming by elevation for the whole plateau. Nevertheless the extremely high elevations (>6000 m) are disproportionately located in the southwestern plateau and Himalayan regions. Qin *et al.* (2009) found maximum warming at around 4800 m in their analysis of warming rates for 2000–2006 based on raw MODIS LST. There was a more stable pattern at the highest elevations (mostly in the Himalayan region)

(~6600 m). Guo *et al.* (2016) predicted maximum warming rates around 4400–5200 m based on high resolution dynamical downscaling simulations. Gao *et al.* (2018) used model simulations to examine future (21st century) patterns of elevation-dependent warming, and projected peak warming around 5000 m associated with snow-albedo feedback, and a decrease above this elevation. Guo *et al.* (2019) used satellite-based 2 m air temperature to reveal a reversal in elevation dependent warming above 4500 m on the TP in recent years. Pepin *et al.* (2019) corrected MODIS LST data to more closely represent air temperature, and analyzed patterns of warming in three mountain ranges across the plateau for 2002–2017. Although some enhanced warming at high elevations was found in the Nyenchen Tanglha and Qilian Mountains, in the central Himalayas the warming changed predominantly to cooling above 6000 m.

Although the cooling in this study appears anomalous in the context of longer term warming, owing to the limitation in the length of the satellite record, it is extremely important not to equate this temporary cooling with longer term change. As satellite records lengthen however, we will be able to extend our approach to understand longer-term tendencies. The present study also addresses the influences of snow-albedo feedback and the surrounding free atmosphere on the pattern of southwestern cooling, but restricts analysis to the local scale. Inter-annual and decadal

variabilities in larger-scale circulation indices such as the North Atlantic Oscillation (NAO) (Liu *et al.*, 2018) and ENSO (Shaman and Tziperman, 2005), have been shown to influence the cryosphere on the Tibetan plateau. They may also therefore show relationships with the southwestern cooling, but further work needs to understand such teleconnections, if they exist, through appreciation of the associated mechanisms.

In summary, we have used comprehensive satellite-based datasets to investigate recent climate change and its causing mechanims on the TP. Although most of the plateau is warming, a recent cooling trend in 2 m air temperature based on SBAT is revealed over the southwestern TP from 2001 to 2015. The cooling is supported by the enhancement of snow-albedo feedback (i.e., more snow and higher surface albedo), linked in turn with a cooling of the surrounding free-atmospheric column and anomalous water vapor transport into the southwestern TP. About 45% of the variance in SBAT can be explained by variance in surface albedo, in turn strongly related to snow cover (coefficient of determination: 0.96), indicating a strong control of the snow-albedo feedback mechanism. The study will be useful for assessing the sustainability of solid water resources over the Himalayan Mountains located in the south-western TP.

Acknowledgments: This research was jointly supported by the National Key R&D Program of China (2016YFA0600704), the National Natural Science Foundation of China (41775076, 41871028), and Youth Innovation Promotion Association CAS. We are indebted to Professor Xiaodong Liu from the Institute of Earth Environment, Chinese Academy of Sciences for his constructive comments and discussions during preparation of this study.

References

Bajracharya, S., Maharjan, S., Shrestha, F., Guo, W., Liu, S., Immerzeel, W. and Shresth, B. (2015) The glaciers of the Hindu Kush Himalayas: current status and observed changes from the 1980s to 2010. *International Journal of Water Resources Development*, 31, 161–173.

Cai, D., You, Q., Fraedrich, K. and Guan, Y. (2017) Spatiotemporal temperature variability over the Tibetan Plateau: Altitudinal dependence associated with the global warming hiatus. *Journal of Climate*, 30, 969–984.

Dee, D., Uppala, S., Simmons, A., Berrisford, P., Poli, P., Kobayashi, S., … and Balmaseda, M. (2011) The ERA-Interim reanalysis: configuration and performance of the data assimilation system. *Quarterly Journal of the Royal*

Meteorological Society, 137, 553–597.

Dimri, A. and Dash, S. (2012) Wintertime climatic trends in the western Himalayas. *Climatic Change*, 111, 775–800.

Dimri, A., Kumar, D., Choudhary, A. and Maharana, P. (2018) Future changes over the Himalayas: mean temperature. *Global and Planetary Change*, 162, 235–251.

Duan, A., Li, F., Wang, M. and Wu, G. (2011) Persistent weakening trend in the spring sensible heat source over the Tibetan Plateau and its impact on the Asian summer monsoon. *Journal of Climate*, 24, 5971–5682.

Gao, X., Wu, J., Shi, Y., Wu, J., Han, Z., Zhang, D., Tong, Y., Li, R., Xu, Y. and Giorgi, F. (2018) Future changes in thermal comfort conditions over China based on multi-RegCM4 simulations. *Atmospheric and Oceanic Science Letters*, 11, 291–299.

Gao, Y., Chen, F., Lettenmaier, D., Xu, J., Xiao, L. and Li, X. (2018) Does elevation-dependent warming hold true above 5000 m elevation? Lessons from the Tibetan Plateau. *npj Climate and Atmospheric Science*, 1, doi:10.1038/s41612-018-0030-z.

Giorgi, F. and Gao, X. (2018) Regional earth system modeling: review and future directions. *Atmospheric and Oceanic Science Letters*, 11, 189–197.

Guo, D. and Wang, H. (2012) The significant climate warming in the northern Tibetan

Plateau and its possible causes. *International Journal of Climatology*, 32, 1775–1781.

Guo, D. and Wang, H. (2013) Simulation of permafrost and seasonally frozen ground conditions on the Tibetan Plateau, 1981-2010. *Journal of Geophysical Research: Atmospheres*, 118, 5216–5230.

Guo, D. and Wang, H. (2016) CMIP5 permafrost degradation projection: a comparison among different regions. *Journal of Geophysical Research: Atmospheres*, 121, 4499–4517.

Guo, D., Sun, J. and Yu, E. (2018) Evaluation of CORDEX regional climate models in simulating temperature and precipitation on the Tibetan Plateau. *Atmospheric and Oceanic Science Letters*, 11, 219–227.

Guo, D., Sun, J., Yang, K., Pepin, N. and Xu, Y. (2019) Revisiting recent elevation-dependent warming on the Tibetan Plateau using satellite-based datasets. *Journal of Geophysical Research: Atmospheres*, doi: 10.1029/2019JD030666.

Guo, D., Yu, E. and Wang, H. (2016) Will the Tibetan Plateau warming depend on elevation in the future? *Journal of Geophysical Research: Atmospheres*, *121*, 3969–3978.

Hall, D., Riggs, G. and Salomonson, V. (1995) Development of methods for mapping global snow cover using moderate resolution imaging spectroradiometer data. *Remote Sensing of Environment*, 54, 127–140.

Hu, Q., Jiang, D. and Fan, G. (2014) Evaluation of CMIP5 Models over the Qinghai-Tibetan Plateau. *Chinese Journal of Atmospheric Sciences*, 38, 924−938.

Huang, F., Ma, W., Wang, B., Hu, Z., Ma, Y., Sun, G., Xie, Z. and Lin, Y. (2017) Air temperature estimation with MODIS data over the northern Tibetan Plateau. *Advances in Atmospheric Sciences*, 34, 650–662.

Immerzeel, W., Van Beek, L. and Bierkens, M. (2010) Climate change will affect the Asian water towers. *Science*, 328, 1382–1385.

IPCC. (2013) Summary for policymakers, in *Climate Change 2013: The Physical Science Basis. Contribution of Working Group I to the Fifth Assessment Report of the Intergovernmental Panel on Climate Change*, Cambridge Univ. Press, Cambridge, U. K.

Jiang, D., Tian, Z. and Lang X. (2016) Reliability of climate models for China through the IPCC Third to Fifth Assessment Reports. *International Journal of Climatology*, 36, 1114−1133.

Jin, L., Ganopolski, A., Chen, F., Claussen, M. and Wang, H. (2005) Impacts of snow

and glaciers over Tibetan Plateau on Holocene climate change: sensitivity experiments with a coupled model of intermediate complexity. *Geophysical Research Letters*, 32, L17709, doi.org/10.1029/2005GL023202.

Kang, S., Xu, Y., You, Q., Flügel, W., Pepin, N. and Yao, T. (2010) Review of climate and cryospheric change in the Tibetan Plateau. *Environmental Research Letters*, 5, 015101.

Kosaka, Y. and Xie, S. (2013) Recent global-warming hiatus tied to equatorial Pacific surface cooling. *Nature*, 501, 403–407.

Li, Q., Liu, X., Zhang, H., Peterson, T. and Easterling, D. (2004) Detecting and adjusting on the temporal inhomogeneity in Chinese mean surface air temperature dataset. *Advances in Atmospheric Sciences*, 21, 260–268.

Li, X., Cheng, G., Jin, H., Kang, E., Che, T., Jin, R., Wu, L., Nan, Z., Wang, J. and Shen, Y. (2008) Cryospheric change in China. *Global and Planetary Change*, 62, 210–218.

Liu, X. and Chen, B. (2000) Climatic warming in the Tibetan Plateau during recent decades. *International Journal of Climatology*, 20, 1729–1742.

Liu, Y., Chen, H., Wang, H. and Qiu, Y. (2018) The impact of the NAO on the delayed break-up date of lake ice over the southern Tibetan Plateau. *Journal of Climate*, 31, 9073–9086.

Ma, Y., Kang, S., Zhu, L., Xu, B., Tina, L. and Yao, T. (2008) Tibetan observation and research platform. *Bulletin of the American Meteorological Society*, 89, 1487–1492.

Maussion, F., Scherer, D., Mölg, T., Collier, E., Curio, J. and Finkelnburg, R. (2014) Precipitation seasonality and variability over the Tibetan Plateau as resolved by the high Asia reanalysis. *Journal of Climate*, 27, 1910–1927.

Pepin, N., Bradley, R., Diaz, H., Baraer, M., Caceres, E., Forsythe, N., Fowler, H., Greenwood, G., Hashmi, M., Liu, X., Miller, J., Ning, L., Ohmura, A., Palazzi, E., Rangwala, I., Schöner, W., Severskiy, I., Shahgedanova, M., Wang, M., Williamson, S. and Yang, D. (2015) Elevation-dependent warming in mountain regions of the world. *Nature Climate Change*, 5, 424–430.

Pepin, N., Deng, H., Zhang, H., Zhang, F., Kang, S. and Yao, T. (2019) An examination of temperature trends at high elevations across the Tibetan Plateau: The use of MODIS LST to understand patterns of elevation-dependent warming. *Journal of Geophysical Research: Atmospheres*, 124, doi.org/10.1029/2018JD029798.

Pepin, N., Maeda, E. and Williams, R. (2016) Use of remotely-sensed land surface temperature as a proxy for air temperatures at high elevations: Findings from a 5000 metre elevational transect across Kilimanjaro. *Journal of Geophysical*

Research: Atmospheres, 121, 9998–10015.

Qin, J., Yang, K., Liang, S. and Guo, X. (2009) The altitudinal dependence of recent rapid warming over the Tibetan Plateau. *Climatic Change*, 97, 321–327.

Qin, J., Yang, K., Liang, S., Zhang, H., Ma, Y., Guo, X. and Chen, Z. (2011) Evaluation of surface albedo from GEWEX-SRB and ISCCP-FD data against validated MODIS product over the Tibetan Plateau. *Journal of Geophysical Research*, 116, D24116, doi:10.1029/2011JD015823.

Rangwala, I. and Miller, J. (2012) Climate change in mountains: a review of elevation-dependent warming and its possible causes. *Climatic Change*, 114, 527–547.

Schneider, U., Andreas, B., Peter, F., Anja, M., Bruno, R. and Markus, Z. (2011) GPCC Full Data Reanalysis Version 6.0 at 1.0°: Monthly Land-Surface Precipitation from Rain-Gauges built on GTS-based and Historic Data. DOI: 10.5676/DWD_GPCC/FD_M_V7_100.

Shaman, J. and Tziperman, E. (2005) The effect of ENSO on Tibetan Plateau snow depth: A stationary wave teleconnection mechanism and implications for the South Asian monsoons. *Journal of Climate*, 18, 2067–207.

Su, F., Duan, X., Chen, D., Hao, Z. and Cuo, L. (2013) Evaluation of the Global Climate Models in the CMIP5 over the Tibetan Plateau. *Journal of Climate*, 26,

3187–3208.

Tang, B., Shrestha, B., Li, Z., Liu, G., Ouyang, H., Gurung, D., Giriraj, A. and Aung, K. (2013) Determination of snow cover from MODIS data for the Tibetan Plateau region. *International Journal of Applied Earth Observation and Geoinformation*, 21, 356–365.

Wan, Z. (2013) MODIS Land Surface Temperature Products Users' Guide. ERI, University of California, Santa Barbara.

Wang, A. and Zeng, X. (2012) Evaluation of multireanalysis products with in situ observations over the Tibetan Plateau. *Journal of Geophysical Research: Atmospheres*, 117, D05102. https://doi.org/10.1029/2011JD016553.

Wang, A. and Zeng, X. (2018) Impacts of internal climate variability on meteorological drought changes in China. *Atmospheric and Oceanic Science Letters*, 11, 78–85.

Waqas, A. and Athar, H. (2018) Recent decadal variability of daily observed temperatures in Hindukush, Karakoram and Himalaya region in northern Pakistan. *Climate Dynamics*, doi.org/10.1007/s00382-018-4557-9.

Xu, W., Ma, L., Ma, M., Zhang, H. and Yuan, W. (2017) Spatial–temporal variability of snow cover and depth in the Qinghai–Tibetan Plateau. *Journal of Climate*, 30, 1521–1533.

Xu, Y., Knudby, A., Shen, Y. and Liu, Y. (2018) Mapping monthly air temperature in the Tibetan Plateau from MODIS data based on machine learning methods. *IEEE Journal of Selected Topics in Applied Earth Observations and Remote Sensing*, 11, 345–354.

Yan, L. and Liu, X. (2014) Has climatic warming over the Tibetan Plateau paused or continued in recent years? *Journal of Earth, Ocean and Atmospheric Sciences*, 1, 13–28.

Yan, Q., Owen, L., Wang, H. and Zhang, Z. (2018) Climate constraints on glaciation over High-Mountain Asia during the last glacial maximum. *Geophysical Research Letters*, 45, 9024–9033.

Yang, K., Wu, H., Qin, J., Lin, C., Tang, W. and Chen, Y. (2014) Recent climate changes over the Tibetan Plateau and their impacts on energy and water cycle: A review. *Global and Planetary Change*, 112, 79–91.

Yao, T., Thompson, L., Mosbrugger, V., Zhang, F., Ma, Y., Luo, T., Xu, B., Yang, X., Joswiak, D., Wang, W., Joswiak, M., Devkota, L., Tayal, S., Jilani, R. and Fayziev, R. (2012a) Third Pole Environment (TPE). *Environmental Development*, 3, 52–64.

Yao, T., Thompson, L., Yang, W., Yu, W., Gao, Y., Guo, X., Yang, X., Duan, K., Zhao, H., Xu, B., Pu, J., Lu, A., Xiang, Y., Kattel, D. and Joswiak, D. (2012b) Different

glacier status with atmospheric circulations in Tibetan Plateau and surroundings. *Nature Climate Change*, 2, 663–667.

You, Q., Kang, S., Aguilar, E. and Yan, Y. (2008) Changes in daily climate extremes in the eastern and central Tibetan Plateau during 1961–2005. *Journal of Geophysical Research*, 113, D07101, doi:10.1029/2007JD009389.

Zou, D., Zhao, L., Sheng, Y., Chen, J., Hu, G., Wu, T., Wu, J., Xie, C., Wu, X., Pang, Q., Wang, W., Du, E., Li, W., Liu, G., Li, J., Qin, Y., Qiao, Y., Wang, Z., Shi, J. and Cheng, G. (2017) A new map of permafrost distribution on the Tibetan Plateau. *The Cryosphere*, 11, 2527–2542.

Figure and table captions

Figure 1. Comparison between mean 2 m air temperatures series from 104 weather stations, satellite-based 2 m air temperature (SBAT), and MODIS LST from station-corresponding satellite pixels. Panels represent annual mean (top), spring, summer, autumn and winter trends. Dashed lines represent regression lines of the corresponding 2 m air temperature series. Linear trends of each series and correlation coefficients (R) between both SBAT and MODIS LST series and air temperature at weather stations are given at the bottom of each panel.

Figure 2. Spatial distribution of trends (°C decade^{-1}) of satellite-based 2 m air temperature (SBAT) (*continuous shading*) and weather station 2 m air temperature (*points*) (left panels) and mean SBAT series over the

southwestern and entire TP (right panels) for annual (top panel), spring, summer, autumn and winter seasons from 2001 to 2015. For the left panels, solid and dashed lines are iso-lines of smoothed topography with labels giving elevation (m). Areas with trends having a significance level exceeding 95% are denoted with "+" sign. The blue box outlines the southwestern TP identified in the text. For the right panels, dashed lines represent regression lines of the corresponding 2 m air temperature series. Linear trends of the temperature series are given at the top of each panel.

Figure 3. Spatial distribution of trends (°C decade^{-1}) of annual and seasonal mean MODIS LST from 2001 to 2015. Solid and dashed lines are iso-lines of the smoothed topography with labels giving elevation (m). Areas with trends having a significance level exceeding 95% are denoted with "+". The blue box outlines the southwestern TP.

Figure 4. Annual 2 m air temperatures series from weather stations Pulan (30.28°N, 81.25°S), Shiquanhe (32.05°N, 80.08°S), and Nielaer (28.18°N, 85.97°S) in the southwestern TP. Dashed lines represent regression lines of the corresponding 2 m air temperature series. Linear trends of the temperature series are given at the bottom of each panel.

Figure 5. Spatial distribution of annual, spring and winter albedo trends (per decade)

(a, c, e) and snow cover trends (% decade^{-1}) (b, d, f) from 2001 to 2015. Areas with trends having a significance level exceeding 95% are denoted with "+". The box outlines the southwestern TP for panels (a)–(e). For panel (f), the box outlines the southwestern TP and Northwest India which is used in Figure 8.

Figure 6. Temporal variation in mean annual, spring and winter satellite-based 2 m air temperature (SBAT), albedo and snow cover series as averaged over the southwestern TP from 2001 to 2015. R is the temporal correlation coefficient between pairs of series. All correlation coefficients exceed a statistical significance level of 95%.

Figure 7. Spatial distribution of snowfall trends (mm hour^{-1} decade^{-1}) across the entire TP for annual, spring and winter seasons from 2001 to 2015. Areas with trends having a significance level exceeding 95% are denoted with "+". The black straight line outlines the southwestern TP.

Figure 8. Elevation profiles of mean annual satellite-based 2 m air temperature (SBAT) trends (*filled circles*) and mean free atmospheric temperature trends (*open circles*), over the southwestern area outlined with the box in Figure 5f. Error bars are based on 95% confidence intervals around the mean. The horizontal dashed line represents the mean 500 hPa level (5500 m above sea

level).

Figure 9. Spatial distribution of trends (*continuous shading*) (°C decade^{-1}) of annual and seasonal ERA-Interim 2 m air temperature from 2001 to 2015. The solid and dashed lines are iso-lines of the smoothed topography with labels giving elevation (m). Areas with trends having a significance level exceeding 95% are denoted with "+". The blue box outlines the southwestern TP.

Figure 10. Spatial distribution of vertically integrated water vapor transport flux trends (kg m^{-1} s^{-1} decade^{-1}) expressed as vectors for annual, spring and winter from 2001 to 2015. Areas with trends exceeding 90% and 95% confidence levels are shown by light and dark shadings, respectively.

Figure 11. Comparison between mean observed 2 m air temperature anomalies (104 weather stations) and area-averaged satellite-based 2 m air temperature (SBAT) anomalies over the entire TP (2001–2015). Dashed lines represent regression lines for the corresponding 2 m air temperature series. The linear trend of each series, correlation coefficient (R), and de-trended correlation coefficient (DR) of the two series are given at the bottom of the panel.

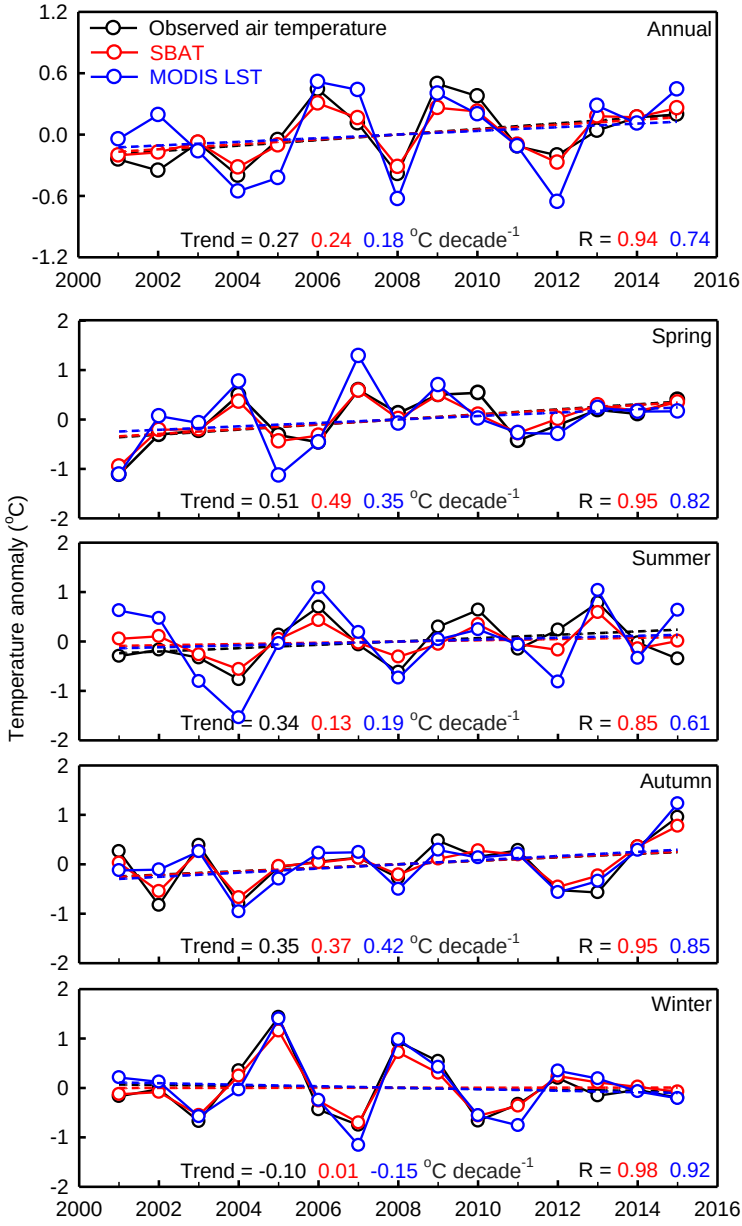

Figure 1. Comparison between mean 2 m air temperatures series from 104 weather stations, satellite-based 2 m air temperature (SBAT), and MODIS LST from station-corresponding satellite pixels. Panels represent annual mean (top), spring, summer, autumn and winter trends. Dashed lines represent regression lines of the corresponding 2 m air temperature series. Linear trends of each series and correlation coefficients (R) between both SBAT and MODIS LST series and air temperature at weather stations are given at the bottom of each panel.

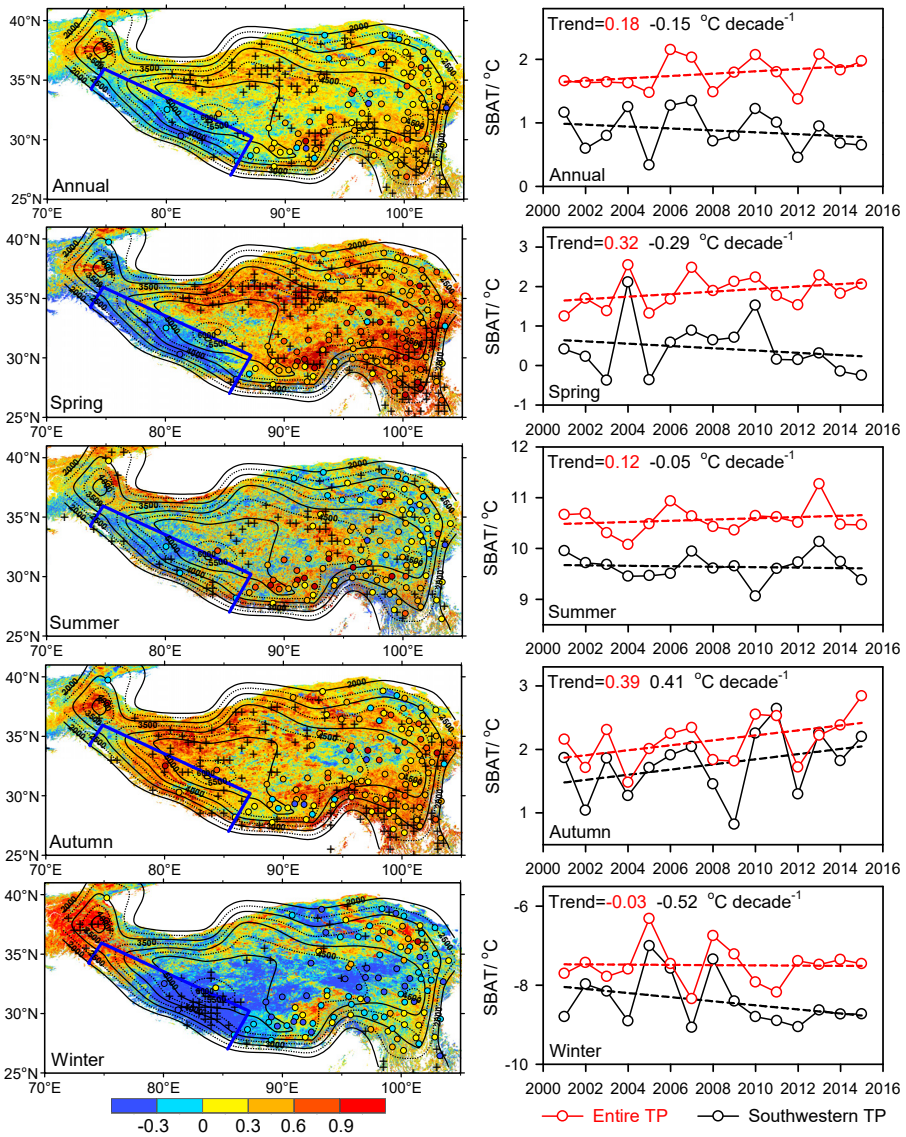

Figure 2. Spatial distribution of trends (°C decade^{-1}) of satellite-based 2 m air temperature (SBAT) (*continuous shading*) and weather station 2 m air temperature (*points*) (left panels) and mean SBAT series over the southwestern and entire TP (right panels) for annual (top panel), spring, summer, autumn and winter seasons from 2001 to 2015. For the left panels, solid and dashed lines are iso-lines of smoothed topography with labels giving elevation (m). Areas with trends having a significance level exceeding 95% are denoted with "+" sign. The blue box outlines the southwestern TP identified in the text. For the right panels, dashed lines represent regression lines of the corresponding 2 m air temperature series. Linear trends of the temperature series are given at the top of each panel.

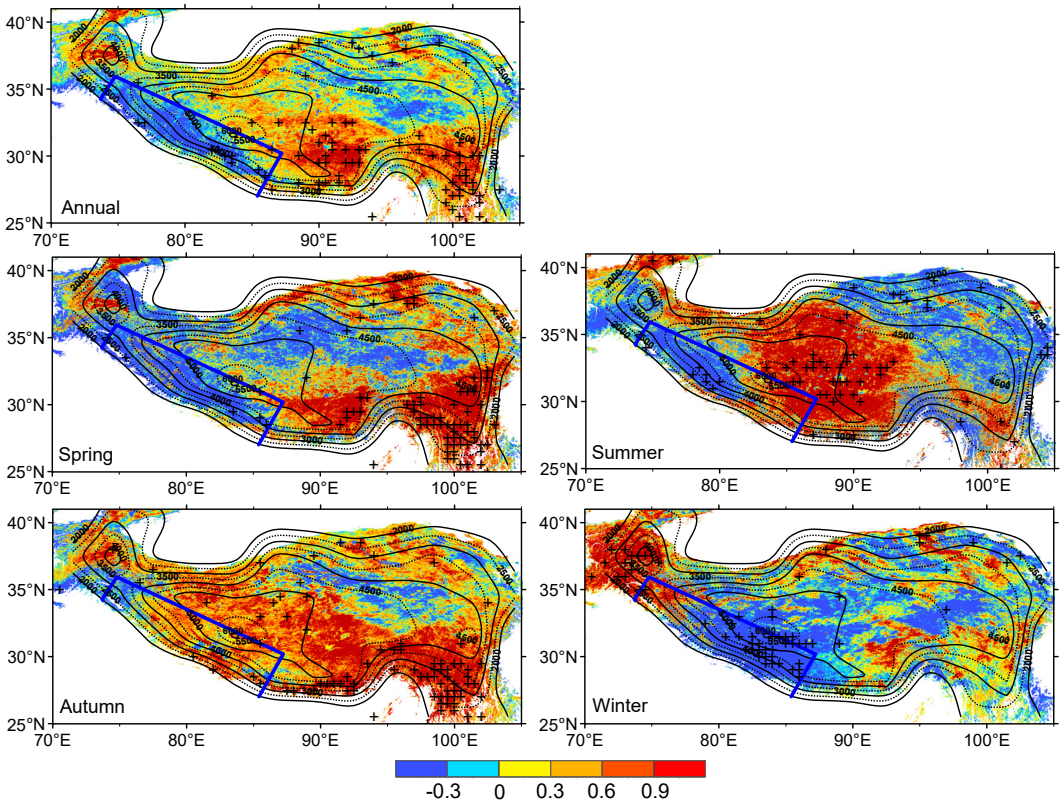

Figure 3. Spatial distribution of trends (°C decade^{-1}) of annual and seasonal mean MODIS LST from 2001 to 2015. Solid and dashed lines are iso-lines of the smoothed topography with labels giving elevation (m). Areas with trends having a significance level exceeding 95% are denoted with "+". The blue box outlines the southwestern TP.

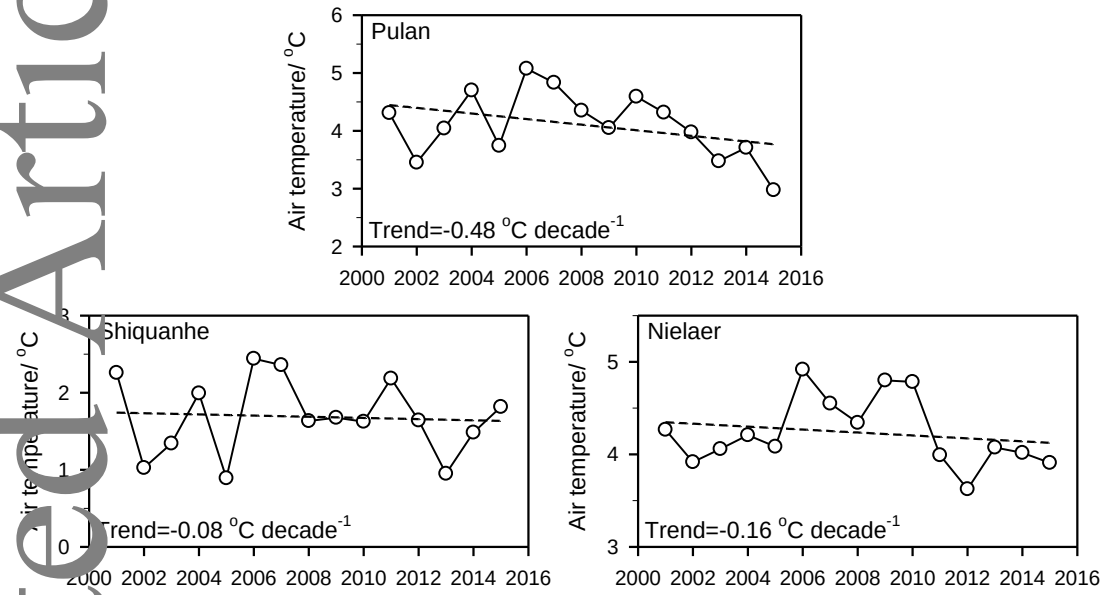

Figure 4. Annual 2 m air temperatures series from weather stations Pulan (30.28 ℃N, 8[illegible] Shiquanhe (32.05 ℃N, 80.08 ℃S), and Nielaer (28.18 ℃N, 85.97 ℃S) in the southwestern TP. Dashed lines represent regression lines of the corresponding 2 m air temperature series. Linear trends of the temperature series are given at the bottom of each panel.

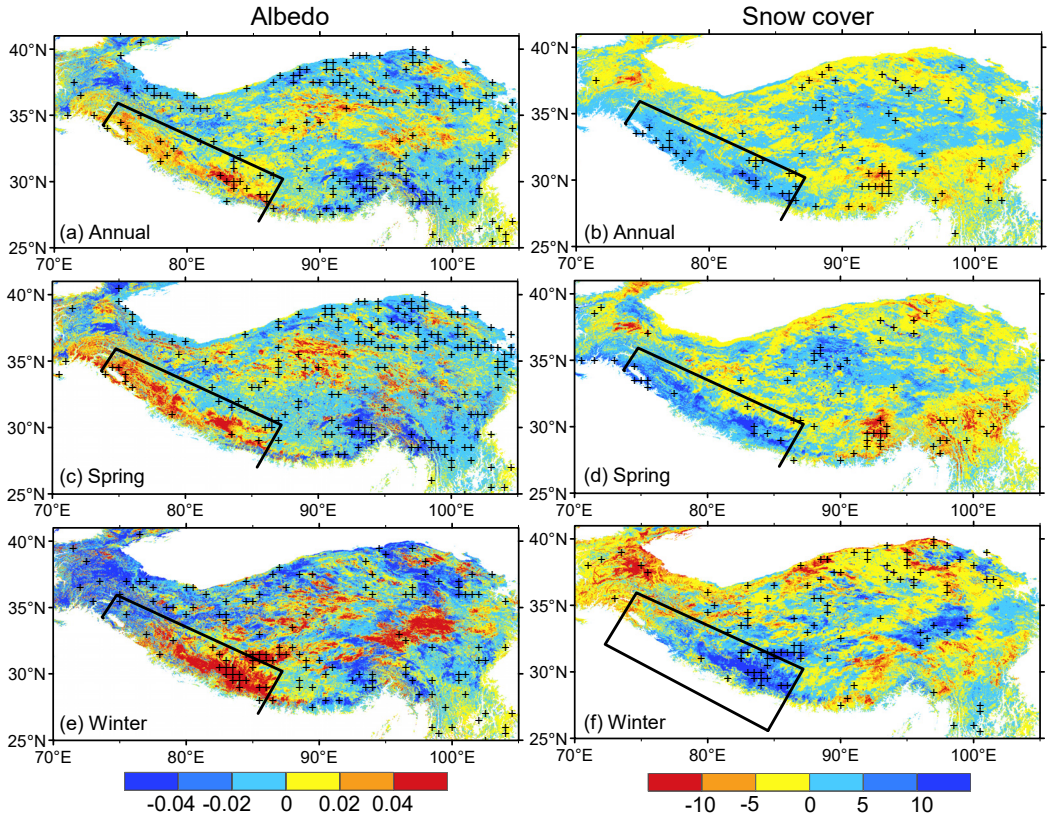

Figure 5. Spatial distribution of annual, spring and winter albedo trends (per decade) (a, c, e) and snow cover trends (% decade^{-1}) (b, d, f) from 2001 to 2015. Areas with trends having a significance level exceeding 95% are denoted with "+". The box outlines the southwestern TP for panels (a)–(e). For panel (f), the box outlines the southwestern TP and Northwest India which is used in Figure 8.

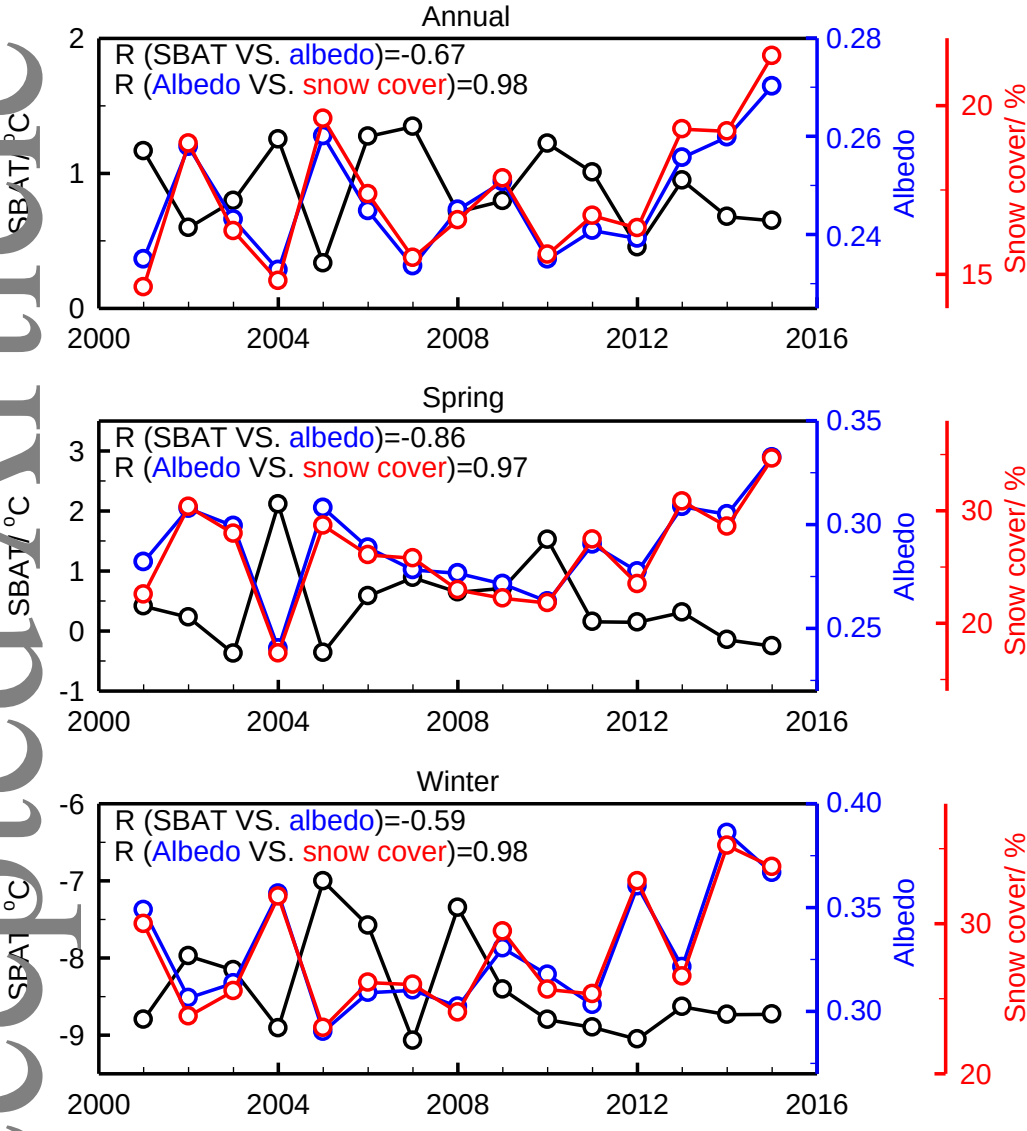

Figure 6. Temporal variation in mean annual, spring and winter satellite-based 2 m air temperature (SBAT), albedo and snow cover series as averaged over the southwestern TP from 2001 to 2015. R is the temporal correlation coefficient between pairs of series. All correlation coefficients exceed a statistical significance level of 95%.

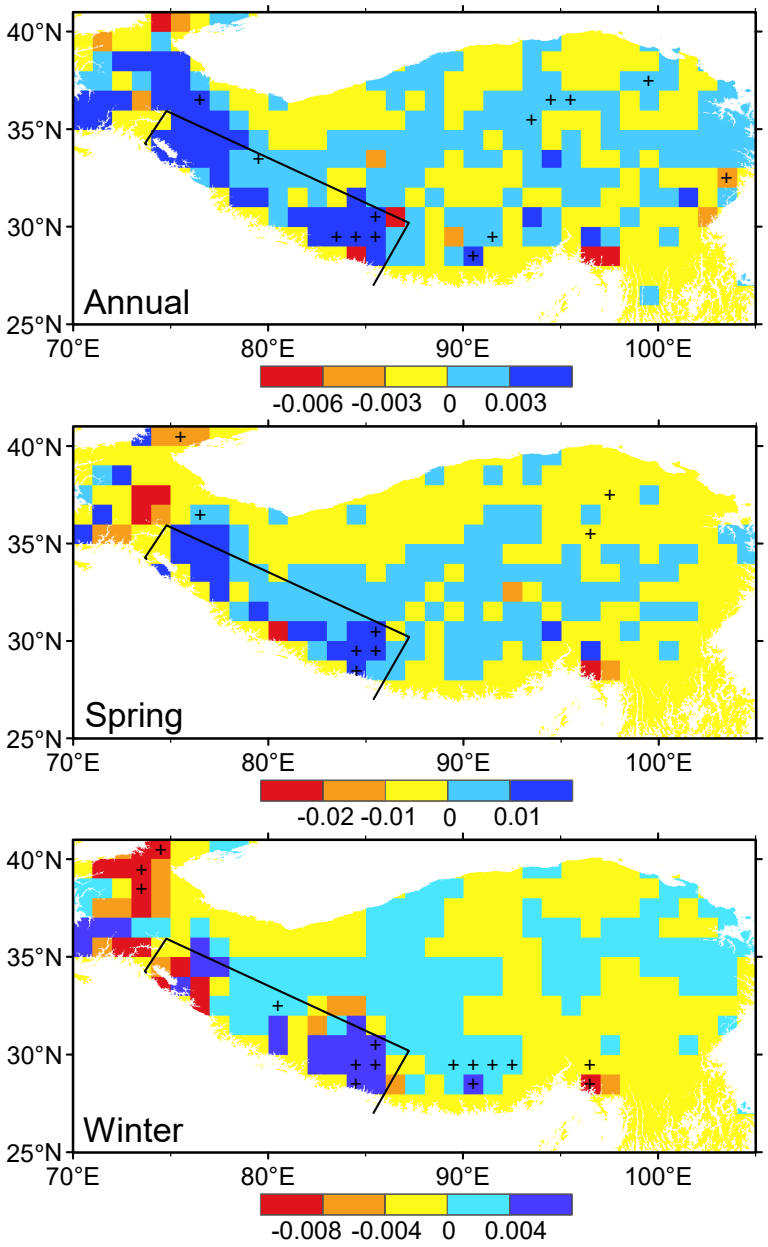

Figure 7. Spatial distribution of snowfall trends (mm hour^{-1} decade^{-1}) across the entire TP for annual, spring and winter seasons from 2001 to 2015. Areas with trends having a significance level exceeding 95% are denoted with "+". The black straight line outlines the southwestern TP.

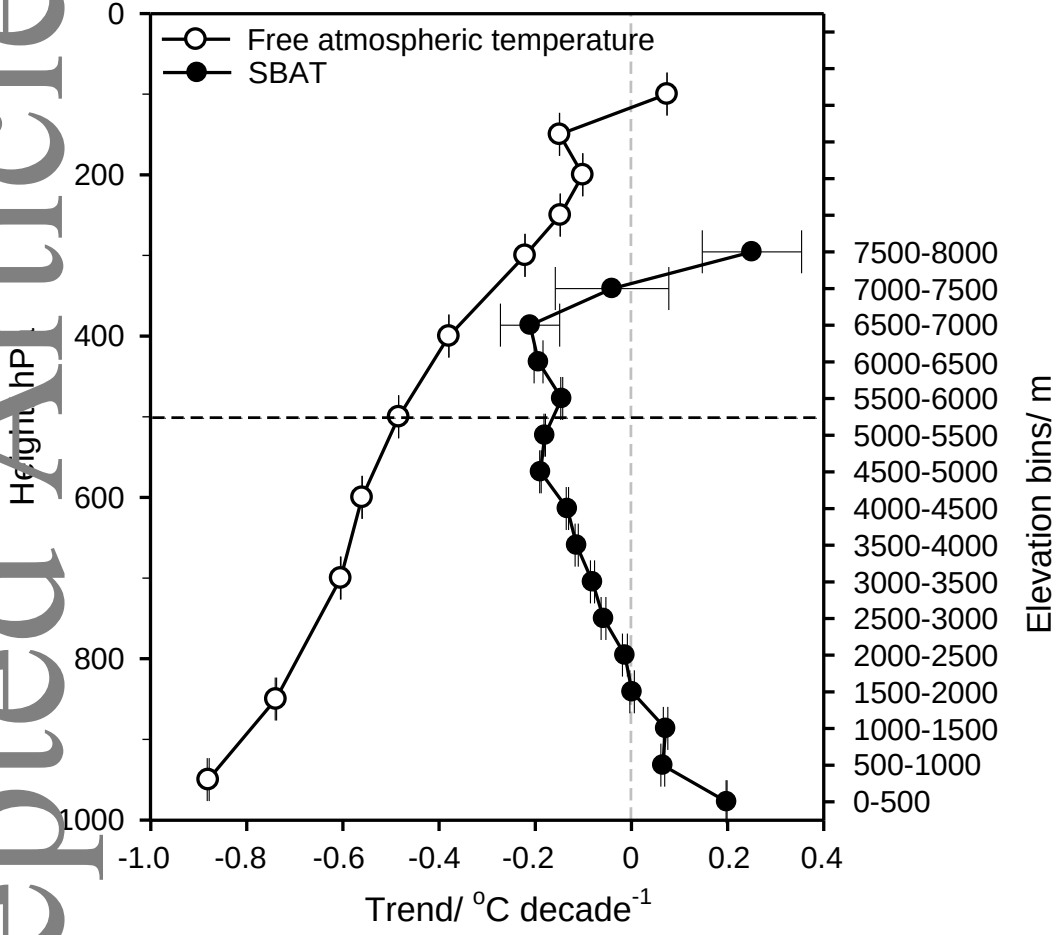

Figure 8. Elevation profiles of mean annual satellite-based 2 m air temperature (SBAT) trends (*filled circles*) and mean free atmospheric temperature trends (*open circles*), over the southwestern area outlined with the box in Figure 5f. Error bars are based on 95% confidence intervals around the mean. The horizontal dashed line represents the mean 500 hPa level (5500 m above sea level).

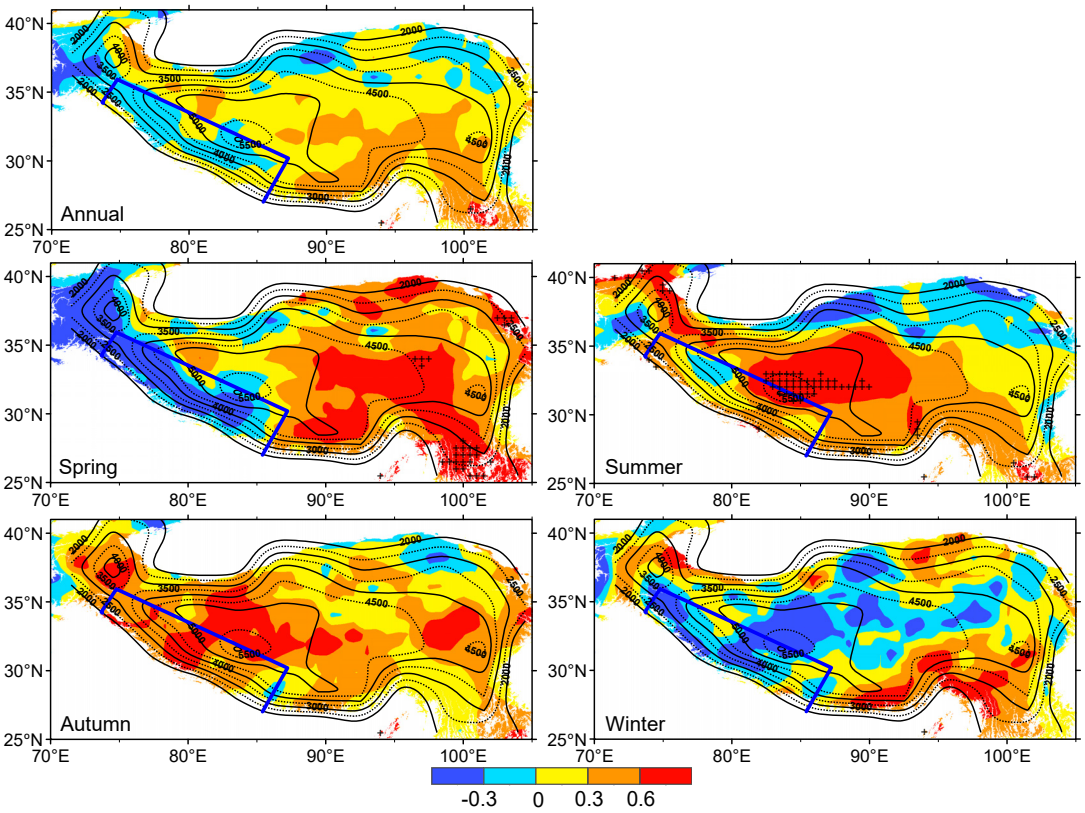

Figure 9. Spatial distribution of trends (*continuous shading*) (°C decade^{-1}) of annual and seasonal ERA-Interim 2 m air temperature from 2001 to 2015. The solid and dashed lines are iso-lines of the smoothed topography with labels giving elevation (m). Areas with trends having a significance level exceeding 95% are denoted with "+". The blue box outlines the southwestern TP.

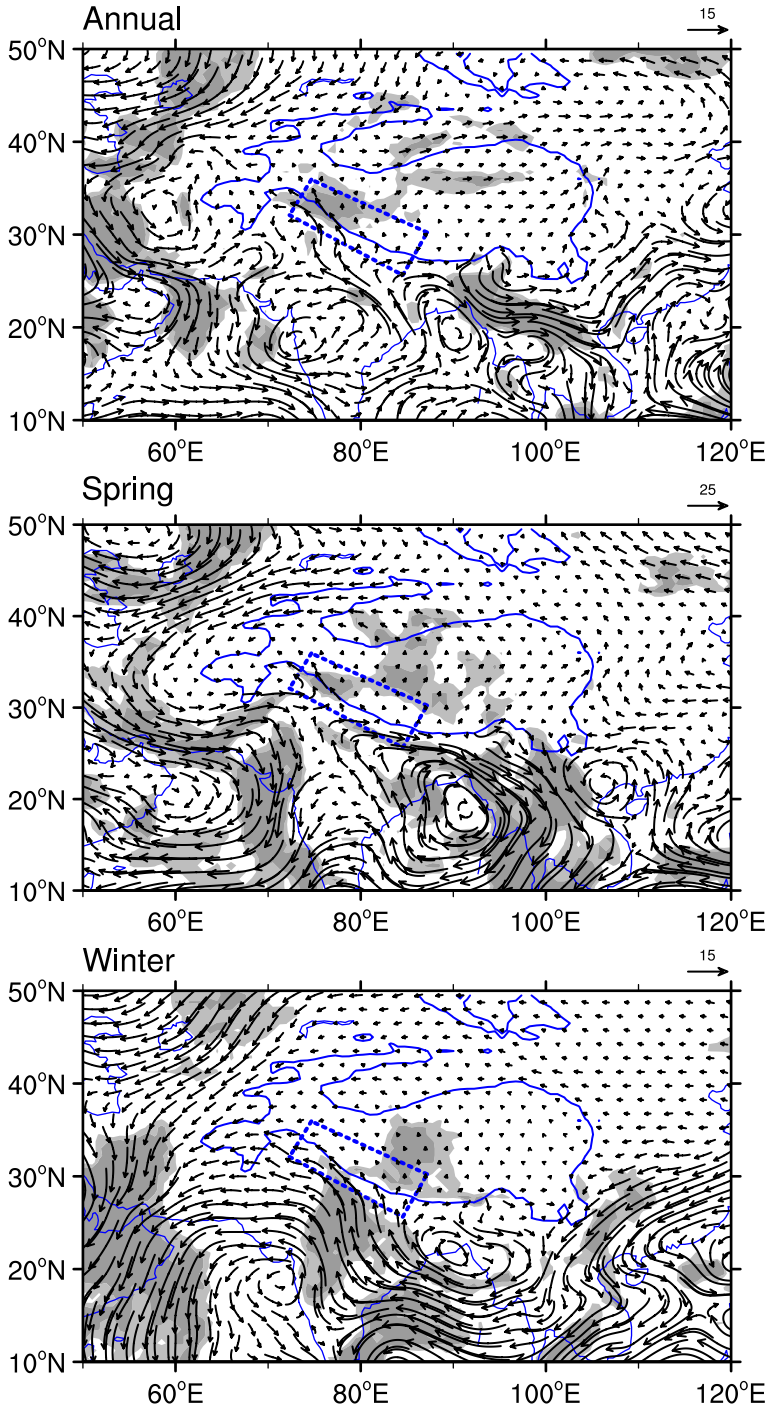

Figure 10. Spatial distribution of vertically integrated water vapor transport flux trends (kg m^{-1} s^{-1} $decade^{-1}$) expressed as vectors for annual, spring and winter from 2001 to 2015. Areas with trends exceeding 90% and 95% confidence levels are shown by light and dark shadings, respectively.

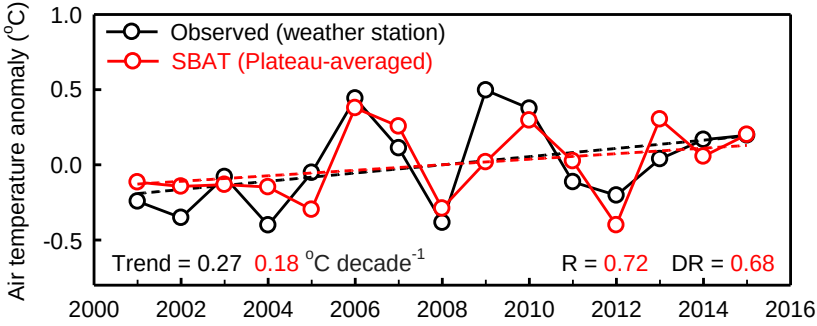

Figure 11. Comparison between mean observed 2 m air temperature anomalies (104 weather stations) and area-averaged satellite-based 2 m air temperature (SBAT) anomalies over the entire TP (2001–2015). Dashed lines represent regression lines for the corresponding 2 m air temperature series. The linear trend of each series, correlation coefficient (R), and de-trended correlation coefficient (DR) of the two series are given at the bottom of the panel.